On the Reduction of MoO_3 to MoO_2: A Path to Control the Particle Size and Morphology

Michael Zoller,[a] Michael O'Sullivan,[b] and Hubert Huppertz*[c]

Abstract: During the reduction of molybdenum trioxide (MoO_3) to metallic molybdenum, the first reduction step yielding molybdenum dioxide as an intermediary product is of crucial importance. In this study, we examined the impact of the parameters reduction temperature, water influx, and potassium content on the hydrogen reduction of this first reaction step. Beginning from the same starting material, the chemical vapor transport mechanism was utilized to yield the phase pure MoO_2. Analyses including powder X-ray diffraction, inductively coupled plasma-mass spectrometry, scanning electron microscopy, and high performance optical microscopy were performed on the product phases. Modulations of the specific surface areas of molybdenum dioxide ranging from 2.28 to 0.41 m^2/g were possible. Furthermore, a distinct shift from small plate-like grains to cuboid-like forms was achieved.

Introduction

Molybdenum trioxide in itself is a crucial material in many ways. Its applications include heterogeneous catalysis[1], where its ability to oxidize selectively is of tremendous importance, and metallurgy, representing the most important starting material in the reduction process to form elemental molybdenum. Molybdenum containing ores can be found in several places around the world (e.g. USA, Canada, Chile)[2]. The most important mineral is molybdenite (MoS_2), which is often extracted as a byproduct of copper production, where it is interspersed in the Chalcopyrite ($CuFeS_2$) ore.[3] The molybdenite is isolated by a two step floatation, turned into molybdenum trioxide by roasting and converted to ammonium heptamolybdate, which in turn is then calcined to yield molybdenum trioxide.[3b,4]

The reduction mechanism to form molybdenum powder in principle follows a two-step process. At first, the molybdenum trioxide is reduced to molybdenum dioxide via a chemical vapor transport at temperatures of 500–700 °C in hydrogen gas. Several thorough studies on the interaction of molybdenum trioxide and hydrogen and on the underlying reduction process can be found in the literature[5].

The second reduction step to molybdenum powder is conducted at 950–1150 °C in dry or humidified hydrogen gas. This step allows for morphological adjustments by carefully setting the humidity (pseudomorphic transformation vs. chemical vapor transport).[6] The morphology of the resulting molybdenum powder is partially dependent on the habitus of the molybdenum dioxide particles, this is especially true when the subsequent reduction undergoes the pseudomorphic transformation route.[7]

Generally, the first reduction step follows the equation $MoO_3 + H_2 \rightarrow MoO_2 + H_2O$, where Mo_4O_{11} is encountered as an intermediary product.[8] For this reason, the reduction is better described by a two step process according to Scheme 1, TP_1 and TP_2 denote the transport phase, presumably $MoO_2(OH)_2$[9]:

The intermediary phase Mo_4O_{11} is known to occur in two modifications, the monoclinic low temperature η- and the orthorhombic high temperature γ-form. During the hydrogen reduction of MoO_3, it is only encountered at reduction temperatures above 450 °C.[9] In earlier investigations, we have reported extensively on several key physical properties of these phases including thermal, magnetic, and spectroscopic traits.[10] The reduction via two transport phases (TP_1 and TP_2) results in a complete loss of the morphological information from MoO_3 to MoO_2. However, the formation of Mo_4O_{11} has a profound impact on the subsequent formation of MoO_2 particles.[7]

Herein, the first reduction step to form molybdenum dioxide from molybdenum trioxide was investigated in consideration of reduction temperature, potassium content, water influx, and sample mass, which in principle corresponds to the

$$MoO_3 \xrightarrow{TP_1} Mo_4O_{11} \xrightarrow{TP_2} MoO_2$$

Scheme 1. Hydrogen reduction of molybdenum trioxide.

[a] M. Zoller
Institute of General, Inorganic, and Theoretical Chemistry
University of Innsbruck
Innrain 80–82, 6020 Innsbruck (Austria)

[b] M. O'Sullivan
Plansee SE
Metallwerk-Plansee-Straße 71, 6600 Reutte (Austria)

[c] Prof. Dr. H. Huppertz
Institute of General, Inorganic, and Theoretical Chemistry
University of Innsbruck
Innrain 80–82, 6020 Innsbruck (Austria)
E-mail: Hubert.Huppertz@uibk.ac.at

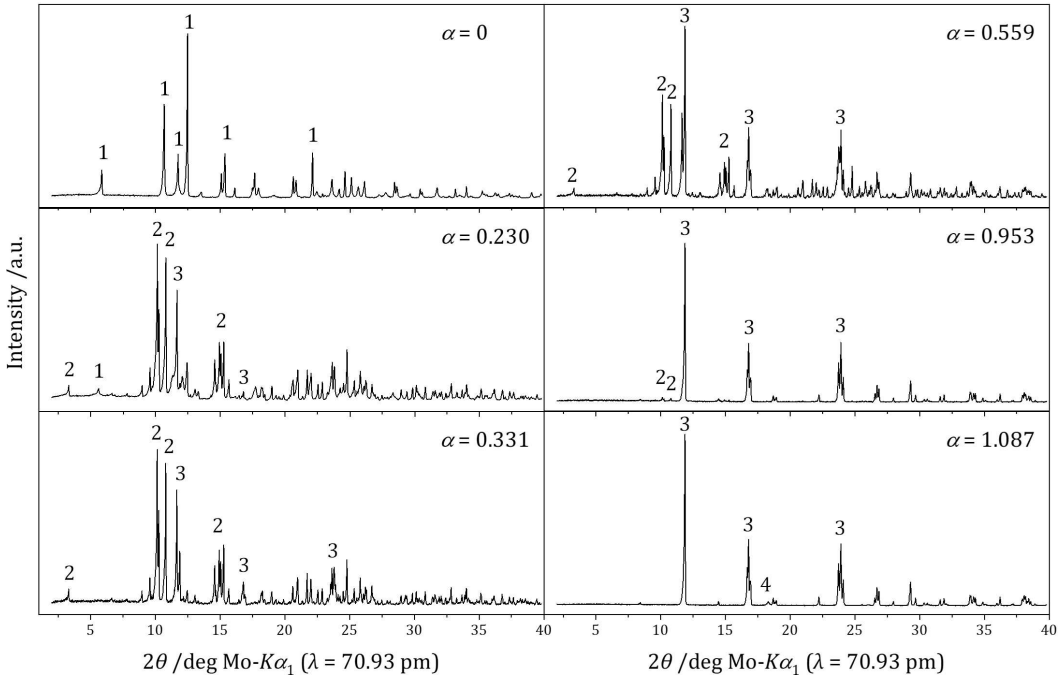

Figure 1. Phase formation during the reduction process (H_2-flow = 0.5 l/min, T = 550 °C, sample mass = 5 g). The highlighted reflections refer to MoO_3 (1), γ-Mo_4O_{11} (2), MoO_2 (3), and Mo (4). The reduction extent α is shown in the top right corner of each illustration.

amount of water developed during the reduction process. A special effort was undertaken to enable the production of molybdenum dioxide powders with predefined morphological parameters, especially with an individual particle size as determined via the BET method.

Results

In a first step, we wanted to verify the partial steps of the whole reduction process, by stopping the reduction in various reduction stages through shifting the gas flow from the reduction gas (hydrogen) to inert gas (argon). The reduction was therefore halted and after cooling to RT, the bulk sample was examined via powder X-ray diffraction (PXRD). The results obtained are depicted in Figure 1.

The reduction extent α relates to the removal of oxygen and is given in the right hand corner of each pattern. The complete reduction ($\alpha \sim 1$) of a 5 g sample of MoO_3 to MoO_2 at 550 °C and a hydrogen flow of 0.5 l/min is performed in 30 mins.

The reduction of large sample amounts shows a significant development of water vapor during the reduction process, consistently measuring dew points (DP) of > 40 °C. To decrease the influence of water vapor, we prepared and reduced 0.5 g samples as well. Dry reduction of 0.5 g samples only showed dew points of ~5 °C, significantly reducing the local dew point (see Figure 2).

To investigate the impact of the potassium content on the reduction of MoO_3, a series of molybdenum trioxide powders

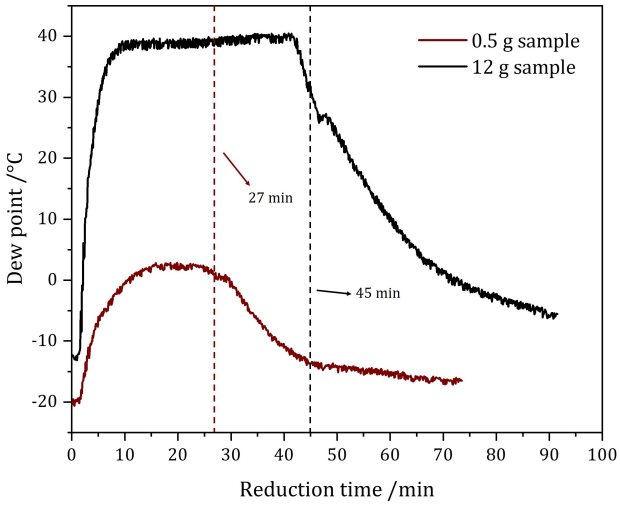

Figure 2. Comparison of the dew point progression of a 12 g and a 0.5 g sample. Reduction starts at t = 0 min and ends at t = 45 and 27 min, respectively.

with potassium contents ranging from 34–160 µg/g were prepared. The progression of the reduction time under otherwise identical conditions is shown in Figure 3 (top) for 12 g and 0.5 g samples. Following the reduction to molybdenum dioxide, the specific surface areas (SSA) of these samples were investigated via the BET method (see Figure 3 bottom). 12 g samples are shown in grey and 0.5 g samples in red (individual values are given in Table 1 and Table 2). In case of the 12 g samples, a decrease from 2.28(7) to 0.41(1) m^2/g coinciding with an increase of the potassium content from 34

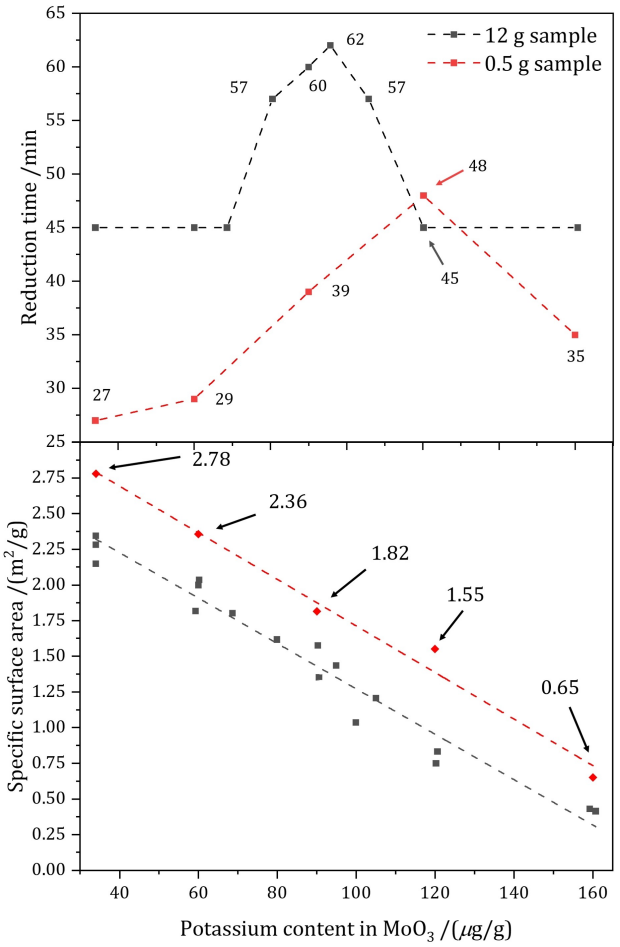

Figure 3. Top: Reduction time in dependence of the potassium content (12 g samples grey; 0.5 g samples red). Bottom: Progression of the specific surface area of reduced MoO_2 with increased potassium content of the original MoO_3 powder (12 g samples grey; 0.5 g samples red; dashed lines are linear fits).

Table 1. Measured specific surface area (m^2/g) of 0.5 g samples reduced at selected conditions.

H_2O-influx /(g/h)	34[a]	60[a]	90[a]	120[a]
0	2.78(7)	2.36(7)	1.82(5)	1.55(5)
0.12	2.24(7)	2.18(7)	1.76(5)	1.41(4)
0.26	2.42(7)	2.36(7)	1.84(6)	1.10(3)
0.67	2.33(7)	2.31(7)	1.70(5)	1.10(3)

[a] potassium content/(μg/g)

Table 2. Specific surface area (SSA) of reduced molybdenum dioxide samples (12 g sample mass).

Potassium content /(μg/g)	SSA /(m^2/g)	Potassium content /(μg/g)	SSA /(m^2/g)
34	2.28(7)	90.6	1.35(4)
34	2.15(6)	94.9	1.42(4)
59.3	1.82(5)	99.9	1.03(3)
60	2.00(6)	105	1.21(4)
60.2	2.04(6)	120.2	0.75(2)
68.6	1.80(5)	120.6	0.83(2)
79.9	1.61(5)	159.2	0.43(1)
90.3	1.58(5)	160.7	0.41(1)

to 159 μg/g is observed. SEM micrographs of selected 12 g and 0.5 g samples containing 34 to 160 μg/g potassium are depicted in Figure 4 and Figure 5. The potassium content following the reduction was determined for samples initially containing 34, 56, and 95 μg/g potassium. The resulting potassium levels measured after the reaction are depicted in Figure 6.

The influence of the water content on the reduction process was studied on 0.5 g samples alongside the potassium content influence in the range 34–120 μg/g potassium and 0–0.67 g/h water influx. The resulting alteration of reduction times is depicted in Figure 7. Subsequently, the specific surface area was measured for all samples (see Figure 8). Scanning electron micrographs of selected samples are depicted in Figure 9.

The hitherto described reductions were conducted at 550 °C to prevent the runaway reaction and to maintain sufficient reaction speeds.[11] To consider a possible temperature influence on the reduction process, reductions at temperatures of 500, 550, 580, 630, and 700 °C were performed.

While the reduction at 500 °C yields the phase pure molybdenum dioxide within 125 mins, the reduction at 700 °C is completed in six mins (see grey squares in Figure 10). The reduction at high temperatures (700 °C) yields purple crystals on the powder bed (see photograph in Figure 11). The samples reduced at 500, 550, 630, and 700 °C were studied via scanning electron microscopy. The resulting micrographs are depicted in Figure 12.

Discussion

During the initial reduction depicted in Figure 1, the MoO_3 (1) powder is reduced to a mixture of the high temperature phase γ-Mo_4O_{11} (2) and MoO_2 (3). The chronological sequence is in good accordance with the reduction steps described by Schulmeyer and Ortner.[6] During the reduction process, γ-Mo_4O_{11} becomes the dominant fraction present in the bulk phase, which is in good accordance with the literature[6,12] as well.

Literature draws the line between the monoclinic low temperature phase η-Mo_4O_{11} and the orthorhombic high temperature phase γ-Mo_4O_{11} at a transformation temperature of 620 °C[13]. Our experiments, however, were conducted at significantly lower temperatures. Only the formation of the high temperature phase γ-Mo_4O_{11} was observed. This behavior is presumably due to the elevated local temperatures caused by the exothermic reduction[11] and is commonly described in the literature [8, 12, 14]. Subsequently, Mo_4O_{11} describes γ-Mo_4O_{11} for brevity.

After the complete reduction to MoO_2, the powder is slowly further reduced to metallic Mo (4). To obtain the phase pure molybdenum dioxide, correct timing is of the essence as prolonged hydrogen flow results in a slow reduction of the molybdenum dioxide to metallic molybdenum ($\alpha > 1$). The further reduction to molybdenum seems to start before all of the MoO_3/Mo_4O_{11} is converted to MoO_2 as evident by the parallel existence of all four phases (see Figure 13). This

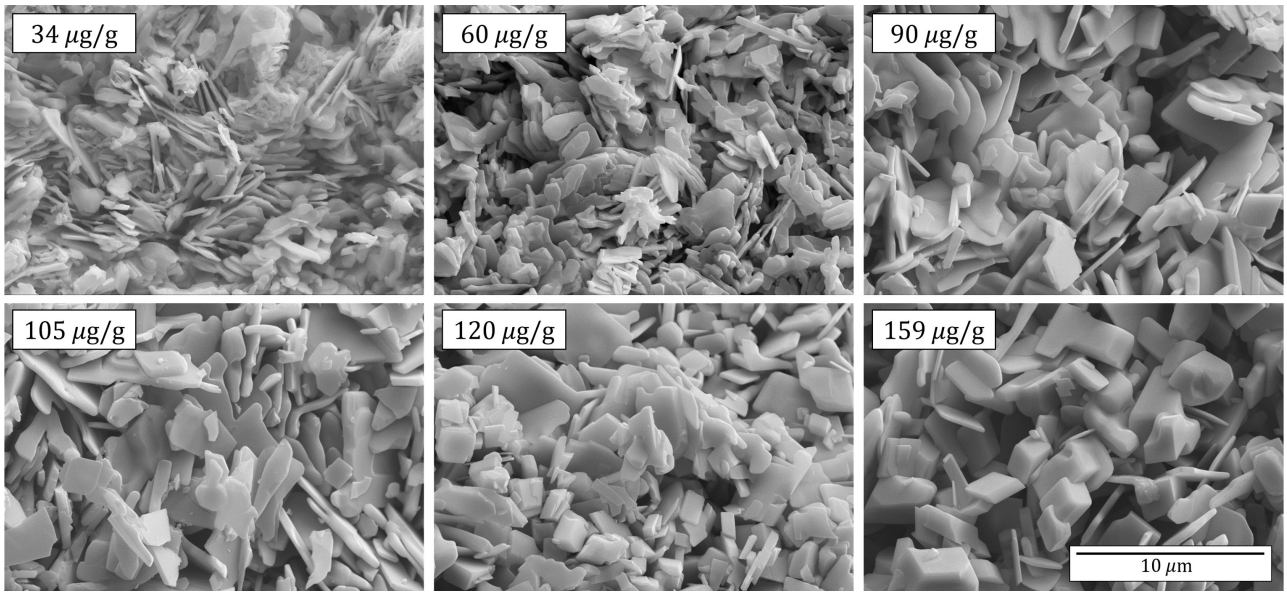

Figure 4. Morphologies of selected MoO_2 samples (sample mass = 12 g). The potassium contents are given in the top left corners. The scale in the bottom right corner applies to all micrographs.

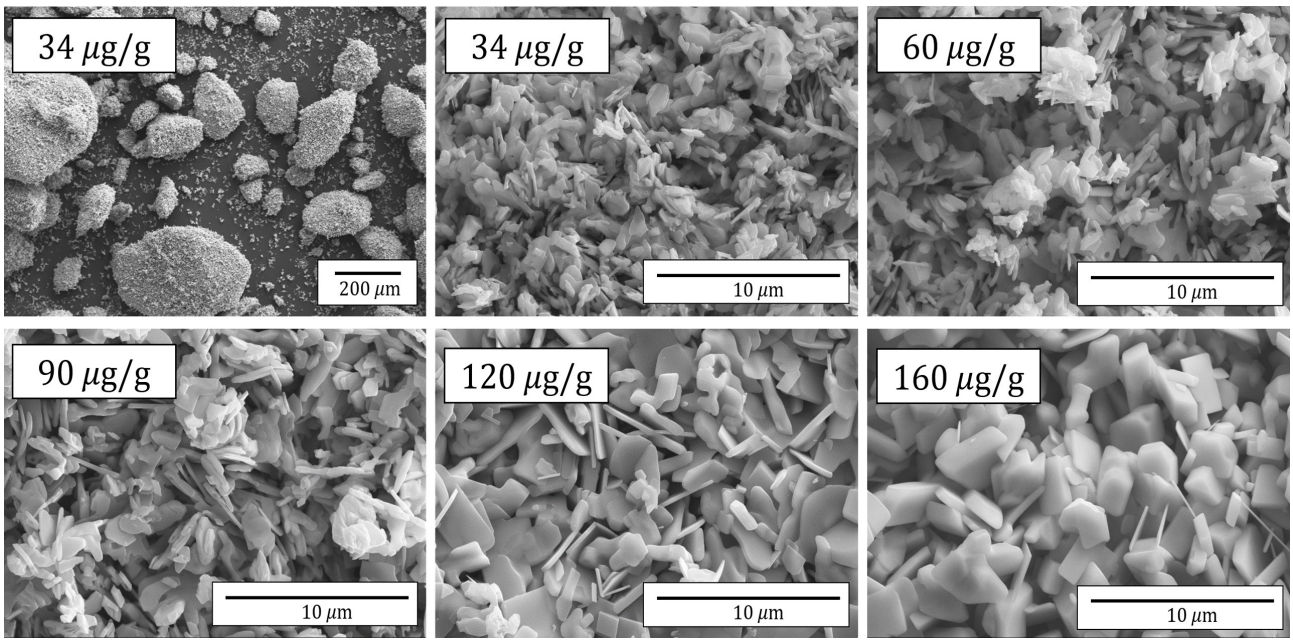

Figure 5. Morphology of selected molybdenum dioxide samples (sample mass = 0.5 g; potassium content in top left corner).

behavior is especially observable for small sample amounts. Although morphological information regarding the individual grains is completely lost, the chemical vapor transport is localized enough to maintain the original particle size and form (compare Figure 14 and Figure 5 top left).

Potassium contents of > 70 μg/g in the 12 g sample result in an initial deceleration of the reduction, as demonstrated in Figure 3 (top; grey squares). However, with continually higher potassium contents, the reduction velocity starts to increase again and the initial reduction velocity is obtained at potassium contents > 120 μg/g, coinciding with a thickening of grain platelets observed in the scanning electron micrographs (see Figure 4).

The reduction of the 0.5 g samples shows a similar trend offset to higher potassium contents (Figure 3 top). It is highly interesting to observe that in the case of the sample containing 120 μg/g potassium, the 12 g sample undergoes a faster reduction than the 0.5 g sample. During the reduction process, the relative potassium concentration rises due to the expulsion of oxygen (overall mass loss of ~11%). The absolute potassium

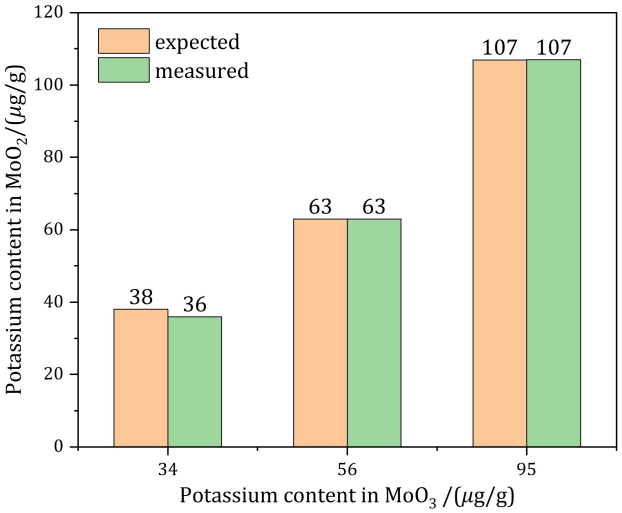

Figure 6. Potassium content of MoO_2 reduced from 34/56/95 µg/g K^+ containing MoO_3 samples.

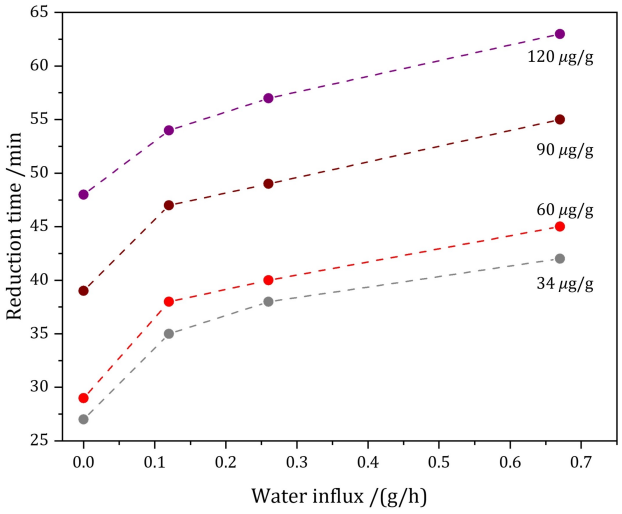

Figure 7. Time to complete the reduction to molybdenum dioxide in dependence of the water influx and potassium content (0.5 g samples T = 550 °C). Potassium contents are shown on the right.

content however, stays unchanged throughout this reduction step. The potassium content measured in the resulting molybdenum dioxide agrees well with the potassium content calculated in line with the overall mass loss caused by the reduction process. This behavior is similar to the results obtained during the reduction of the higher homologue WO_3 as described by Haubner et al.[15], where the alkali supplement only dissipates at T > 800 °C.

The specific surface area of 0.5 g (red) and 12 g (grey) samples in Figure 3 (bottom) decreases with increasing potassium contents. Scanning electron micrographs of 12 g samples depicted in Figure 4 show the transition from small platelets as described by Schulmeyer and Ortner[6] (top left) to large cuboid like particles (bottom right) caused by the increasing potassium content. The overall reaction seems to follow a chemical vapor

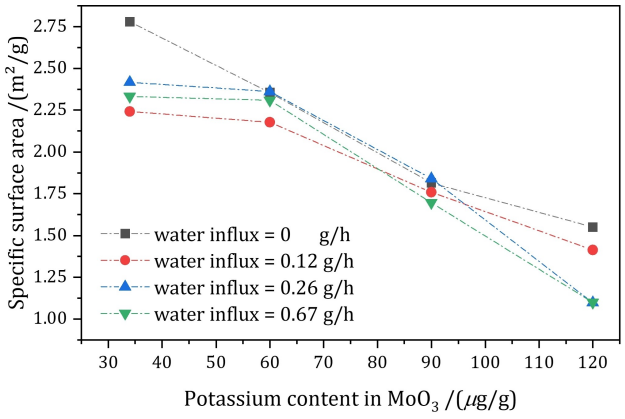

Figure 8. Impact of potassium content on the specific surface area of 0.5 g samples reduced at different water influxes.

transport (CVT) process, where all morphological information of the initial powder, except for particle size, is lost in the reduction process as described in the literature[6]. SEM micrographs of 0.5 g samples with potassium contents ranging from 34 to 160 µg/g depicted in Figure 5 show a likewise morphology compared to the 12 g samples. With increasing potassium content, the overall particle size increases, yielding large platelet/cuboid like structures.

Water vapor is inherently produced throughout the reduction in significant amounts and has a profound impact on the reduction. Increasing the dew point by raising the amount of water inserted into the gas stream leads to a decrease in reduction rate, i.e. the time to complete the reduction to molybdenum dioxide is steadily increased (see Figure 7). The relative decrease in reduction speed by increasing the water influx is not influenced by the potassium content (e.g. relative trend is identical but offset). Table 1 shows the impact of water influx on the specific surface area of 0.5 g samples at different potassium levels and is depicted in a graphical format in Figure 8. The addition of water to the reduction gas causes no clear impact on the specific surface area of the resulting powders, at least not in the range tested. However, smaller sample masses corresponding to lower dew points resulted in a clear shift to higher specific surface areas (see Figure 3 bottom). While the overall trend is unchanged, the specific surface areas are offset by approximately 0.4 m^2/g. Still, while the specific surface area decreases with higher water influx, the particle morphology remains unaltered. Comparing the SEM micrographs in Figure 9 shows that the grain habitus is dominated by the potassium content and the variation in water influx only yields changes in the overall grain size.

Elevating the reduction temperature from 550 to 580 °C yields higher specific surface areas (see red squares in Figure 10). However, with further temperature increase (630 and 700 °C), considerably lower specific surface area values (e.g. 0.91(3) m^2/g at 700 °C) are obtained. At high temperatures, we have observed a behavior of agglomeration of the powder, which is caused by a partial melting of MoO_3 and Mo_4O_{11} as described in the literature[16] and results in a decrease of the

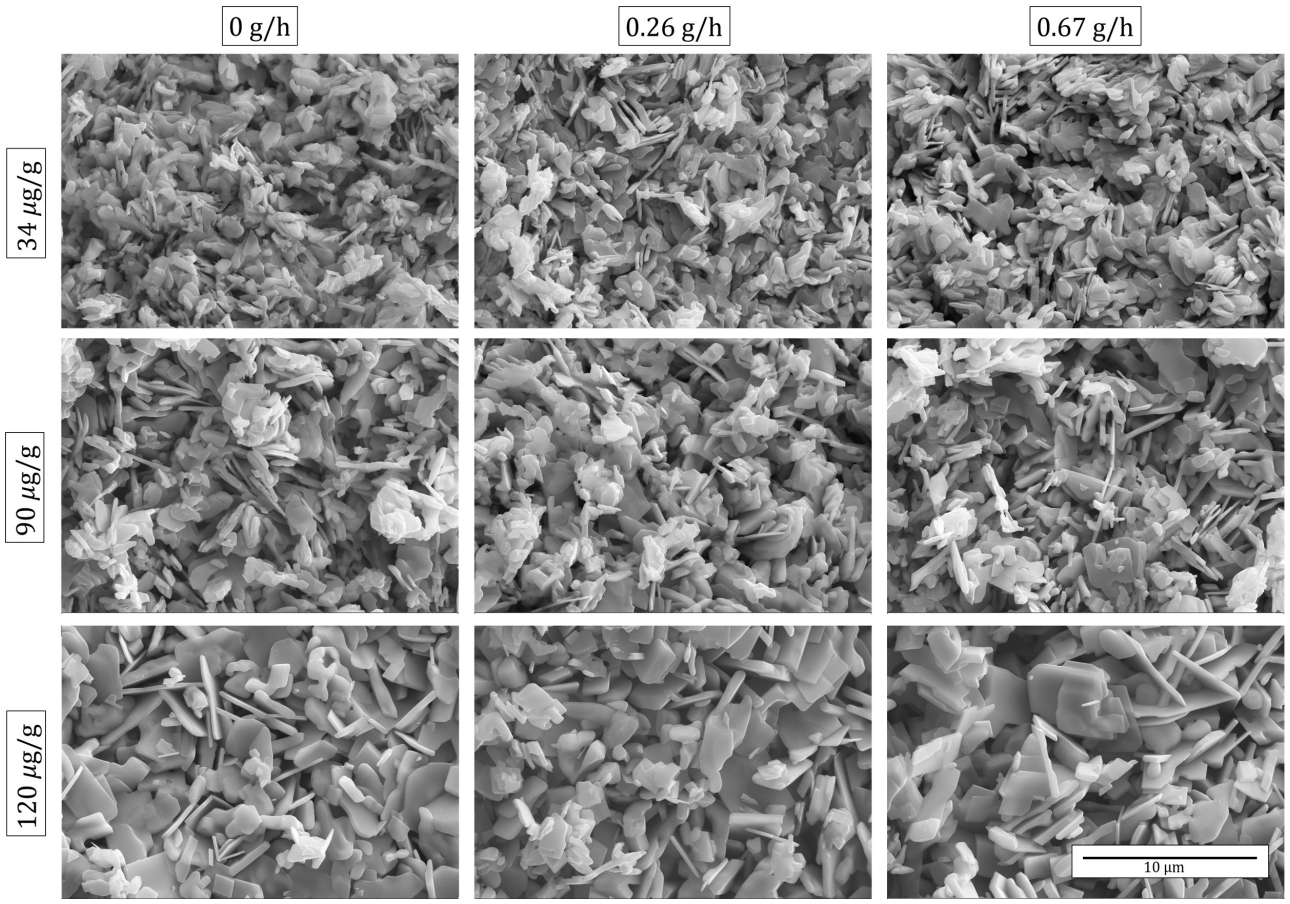

Figure 9. Morphological evolution of 0.5 g samples reduced at different levels of water influx (potassium content 34/90/120 µg/g). The scale in the bottom right corner applies to all micrographs.

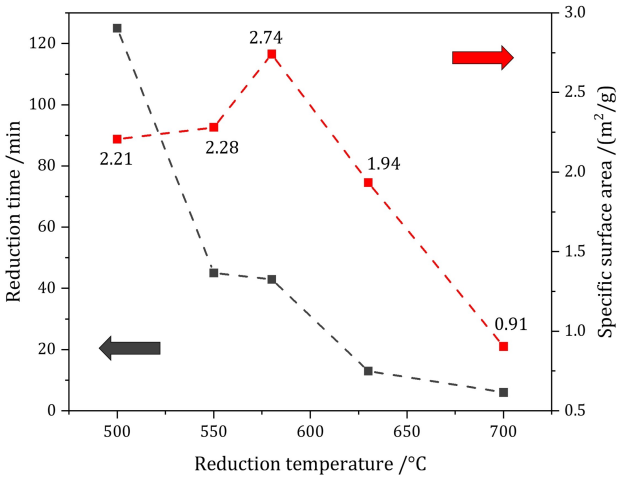

Figure 10. Temperature dependent evolution of the reduction time (grey) and specific surface area (red) of a 12 g sample.

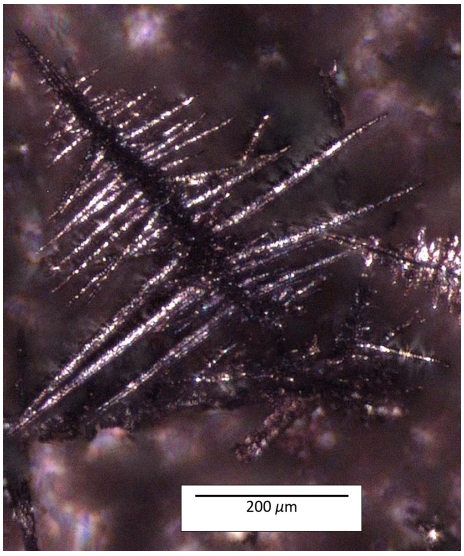

Figure 11. Photograph of a molybdenum dioxide crystal deposited on the powder bed.

measured specific surface areas. At a reduction temperature of 700 °C, the sublimation of MoO_3 during the reduction process becomes an influencing factor as well. MoO_3 sublimes and redeposits on the surface of the powder and is subsequently reduced to MoO_2, yielding purple needle shaped crystals of MoO_2 on top of the compacted powder bed (see Figure 11).

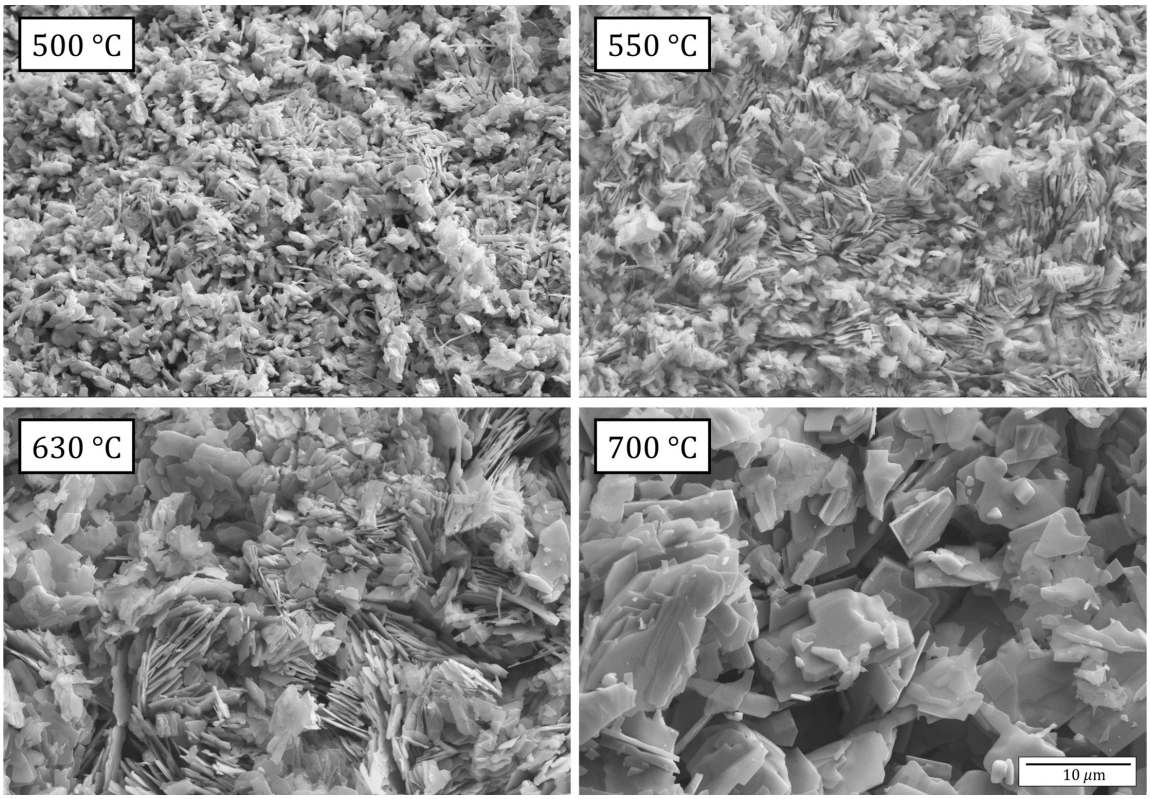

Figure 12. Scanning electron micrographs of molybdenum dioxide samples reduced at different temperatures (potassium content = 34 μg/g). The scale in the bottom right corner applies to all micrographs.

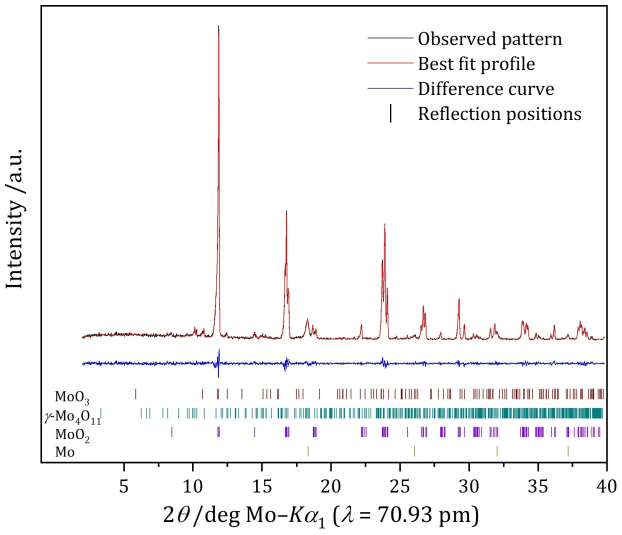

Figure 13. Sample of partially reduced molybdenum trioxide with parallel existence of MoO_3 (~2 w%), γ-Mo_4O_{11} (~4 w%), MoO_2 (~90 w%) and Mo (~4 w%) (sample mass = 100 mg, T = 550 °C).

SEM micrographs depicted in Figure 12 show a growth in size of the platelet structure associated with higher temperatures.

Although the sample reduced at 700 °C has a similar specific surface area as the sample shown in Figure 4 (550 °C, 120 μg/g K^+), the morphology is inherently different. The sample reduced at 700 °C shows irregularly sized, large platelets prone to agglomeration. By contrast, the 120 μg/g potassium sample reduced at 550 °C is dominated by small and well defined cuboids interspersed by larger platelet structures.

Conclusion

The hydrogen reduction of molybdenum trioxide to molybdenum dioxide is governed by several key parameters. The potassium content of the sample is of crucial importance with higher values resulting in lower specific surface areas and bulkier/larger grains. Adjustments of the specific surface area ranging from 2.28 to 0.41 m^2/g were possible. The specific surface area is furthermore lowered by increasing the amounts of intrinsically produced water vapor (e.g. high vs. low sample mass). The specific surface area of the resulting sample can further be controlled by optimizing the reduction temperature. The maximum specific surface area was achieved at T = 580 °C. Further increase of the reduction temperature results in a significant sublimation of molybdenum trioxide and agglomeration of the sample, resulting in decreased specific surface areas. All reductions obeyed the chemical vapor transport mechanism, which however was localized enough to produce samples retaining the initial particle size of the starting material.

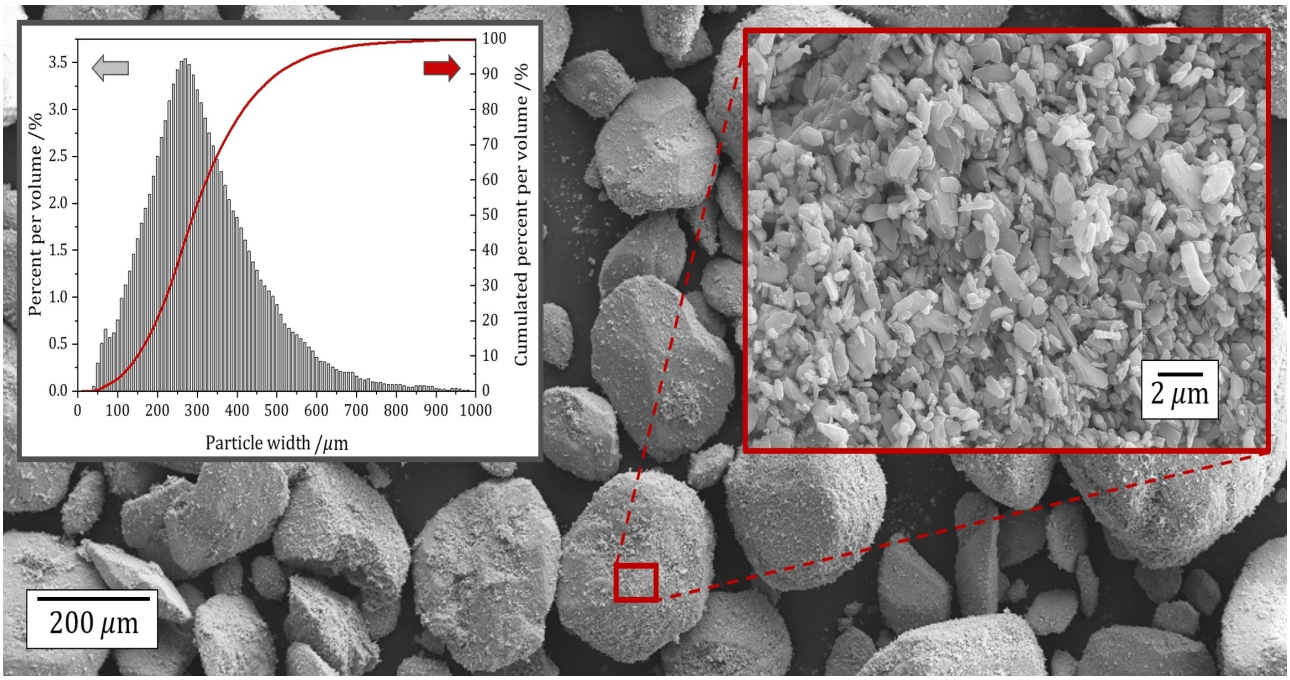

Figure 14. Morphology of the molybdenum trioxide sample used throughout the investigations. The particle distribution is depicted in the top left corner.

Experimental Section

Pure molybdenum trioxide (MoO_3) powder, supplied by Molymet S.A. (San Bernardo, Chile), was used for the experiments. Scanning electron micrographs of the original material are depicted in Figure 14. The typical particles range in size from 50 to 500 μm, with a particle distribution according to the parameters d(0.1) = 130 μm, d(0.5) = 258 μm, and d(0.9) = 452 μm. The native potassium (K^+) content of the powder is 34 μg/g and the specific surface area was determined as 1.82(5) m^2/g. According to the experiments described before, samples with higher potassium content were prepared by addition of a 100 μg/g potassium containing standard solution (prepared from K_2MoO_4), mixing of the solution and powder, and subsequent evaporation of the residual water in a kiln at 90 °C.

To verify the completion of the reduction to MoO_2, the obtained powder was analyzed via X-ray powder diffraction. For this, the sample was thoroughly ground in an agate mortar and placed between two polyacetate foils. The sample was measured utilizing a STOE Stadi P diffractometer with monochromatized Mo-$K\alpha_1$ radiation (λ = 70.93 pm; curved Ge(111) monochromator). The diffraction intensities were collected by a Mythen2 1 K microstrip detector with 1280 strips (Dectris, Baden-Daettwil, Switzerland).

The specific surface area (SSA) was measured by employing the multipoint Brunauer-Emmet-Teller method (3P micro, 3P Instruments GmbH & Co. KG, Odelzhausen, Germany). Measurements of small sample masses with small specific surface areas were possible by using krypton as the adsorption gas throughout our investigations.

Morphological characterizations of the obtained samples were performed by a scanning electron microscope (ZEISS ULTRA PLUS, Carl Zeiss AG, Oberkochen, Germany). In addition, investigations via ICP-MS (inductively coupled plasma-mass spectrometry) to determine the potassium content were conducted for several selected samples.

Photographs of selected samples were recorded utilizing the Keyence VHX-970F (KEYENCE International, Mechelen, Belgium) digital microscope equipped with a high performance 50–500× magnification, ring illumination, and 3D image capturing software.

The reduction experiments were conducted in a split tube furnace with three separate heating zones (HZS 12/600, Carbolite Gero GmbH & Co. KG, Neuhausen, Germany). A fused silica tube (Ø = 40 mm) containing the sample in a fused silica boat was placed in the center of the furnace. To humidify the gas flow, a controlled evaporation mixer (CEM, Bronkhorst High-Tech B.V., AK Ruurlo, The Netherlands) coupled to two mass flow controllers (MFC; both Bronkhorst High-Tech B.V., AK Ruurlo, The Netherlands) regulating the argon and hydrogen gas flow, and a liquid flow meter (LFM, Bronkhorst High-Tech B.V., AK Ruurlo, The Netherlands) to measure the water input, were used. Evaporation of the liquid phase in the CEM was conducted at 130 °C. To verify the set water influx, a dew point (DP) sensor (Michell Instruments GmbH, Friedrichsdorf, Germany) was employed. To prevent condensation of water in the pipes, a heating system set to 130 °C was installed between the CEM and the dew point sensor. The overall experimental reduction setup with the general preparation, reaction, and analysis steps is depicted in Figure 15. The heated pipes are shown in black, water containing pipes in blue and unheated gas pipes in grey.

Acknowledgements

The authors are very grateful to Günther Mitterndorfer for countless hours spent in helping to prepare the herein used apparatus. The authors thank Barbara Votik for the preparation of all glassware, Prof. Dr. Julia Kunze-Liebhäuser for the helpful input regarding the construction of the herein used apparatus. Further thanks are due to Assoc.-Prof. Dr. Clivia Hejny for the access to the digital microscope situated at the Institute of

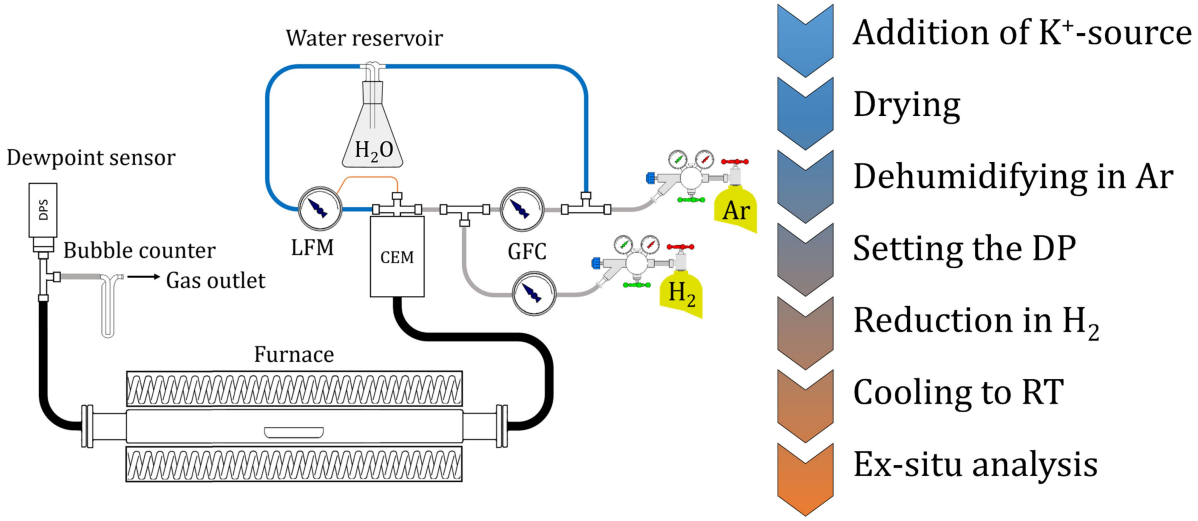

Figure 15. Schematic diagram of the experimental setup for the reduction process (left) and flow chart of the syntheses (right).

Mineralogy and Petrography (University of Innsbruck). The authors thank Dr. Norbert Köpfle for the ICP-MS measurements and gratefully acknowledge the support of Plansee SE (Reutte/Austria).

Conflict of Interest

The authors declare no conflict of interest.

Keywords: hydrogen reduction · molybdenum oxide · potassium · powder diffraction · scanning electron microscopy

[1] a) J. Haber, E. Lalik, *Catal. Today* **1997**, *33*, 119–137; b) J. C. Védrine, *Chin. J. Catal.* **2019**, *40*, 1627–1636.
[2] A. F. Holleman, E. Wiberg, N. Wiberg, *Lehrbuch der Anorganischen Chemie*, De Gruyter, Berlin, **2007**, 1582–1606.
[3] a) N. N. Greenwood, A. Earnshaw, *Chemie der Elemente*, VCH, Weinheim, **1990**, 1288–1334; b) A. Ansari, M. Pawlik, *Miner. Eng.* **2007**, *20*, 609–616.
[4] a) M. Wang, X. Wang, *Hydrometallurgy* **2010**, *102*, 50–54; b) K. Jiang, Y. Wang, X. Zou, L. Zhang, S. Liu, *JOM* **2012**, *64*, 1285–1289; c) S. Singh, M. Chetty, J. Juneja, J. Sehra, C. Gupta, *Miner. Eng.* **1988**, *1*, 337–342.
[5] a) A. Borgschulte, O. Sambalova, R. Delmelle, S. Jenatsch, R. Hany, F. Nüesch, *Sci. Rep.* **2017**, *7*, 40761; b) E. Lalik, W. I. David, P. Barnes, J. F. Turner, *J. Phys. Chem.* **2001**, *B105*, 9153–9156; c) J. Chen, Q. Wei, *Int. J. Appl. Ceram. Technol.* **2017**, *14*, 1020–1025.
[6] W. V. Schulmeyer, H. M. Ortner, *Int. J. Refract. Met. Hard Mater.* **2002**, *20*, 261–269.
[7] X. Wang, J. Liu, F. Zhuang, H. Zhao, L. Jing, *Metall. Mater. Trans.* **2010**, *B41*, 1067–1073.
[8] J. Dang, G.-H. Zhang, K.-C. Chou, R. G. Reddy, Y. He, Y. Sun, *Int. J. Refract. Met. Hard Mater.* **2013**, *41*, 216–223.
[9] G.-D. Sun, G.-H. Zhang, X.-P. Ji, J.-K. Liu, H. Zhang, K.-C. Chou, *Int. J. Refract. Met. Hard Mater.* **2019**, *80*, 11–22.
[10] M. Zoller, R. Bubnova, Y. Biryukov, E. Haussühl, R. Pöttgen, O. Janka, S. Penner, C. Praty, H. Fitzek, J. Winkler, *Z. Kristallogr.* **2020**, *235*, 143–155.
[11] S. Luidold, H. Antrekowitsch, *JOM* **2007**, *59*, 20–26.
[12] E. Lalik, *Catal. Today* **2011**, *169*, 85–92.
[13] L. Kihlborg, *Acta Chem. Scand.* **1959**, *13*, 954–962.
[14] T. Leisegang, A. Levin, J. Walter, D. Meyer, *Cryst. Res. Technol.* **2005**, *40*, 95–105.
[15] R. Haubner, W. Schubert, E. Lassner, B. Lux, *11th Plansee Seminar Proc.* **1985**, *2*, 69–97.
[16] R. K. Enneti, T. A. Wolfe, *Int. J. Refract. Met. Hard Mater.* **2012**, *31*, 47–50.

Manuscript received: September 18, 2021
Accepted manuscript online: October 21, 2021
Version of record online: November 16, 2021